Structure
Article

Evolution of Structure and Mechanistic Divergence in Di-Domain Methyltransferases from Nematode Phosphocholine Biosynthesis

Soon Goo Lee[1] and Joseph M. Jez[1,*]
[1]Department of Biology, Washington University in St. Louis, One Brookings Drive, Campus Box 1137, St. Louis, MO 63130, USA
*Correspondence: jjez@biology2.wustl.edu
http://dx.doi.org/10.1016/j.str.2013.07.023

SUMMARY

The phosphobase methylation pathway is the major route for supplying phosphocholine to phospholipid biosynthesis in plants, nematodes, and *Plasmodium*. In this pathway, phosphoethanolamine N-methyltransferase (PMT) catalyzes the sequential methylation of phosphoethanolamine to phosphocholine. In the PMT, one domain (MT1) catalyzes methylation of phosphoethanolamine to phosphomonomethylethanolamine and a second domain (MT2) completes the synthesis of phosphocholine. The X-ray crystal structures of the di-domain PMT from the parasitic nematode *Haemonchus contortus* (HcPMT1 and HcPMT2) reveal that the catalytic domains of these proteins are structurally distinct and allow for selective methylation of phosphobase substrates using different active site architectures. These structures also reveal changes leading to loss of function in the vestigial domains of the nematode PMT. Divergence of function in the two nematode PMTs provides two distinct antiparasitic inhibitor targets within the same essential metabolic pathway. The PMTs from nematodes, plants, and *Plasmodium* also highlight adaptable metabolic modularity in evolutionarily diverse organisms.

INTRODUCTION

Parasitic nematodes are a major cause of human health problems worldwide, especially in developing regions of Africa, Asia, and the Americas. In humans, an estimated one billion people are infected with nematode parasites (i.e., *Ascaris*, *Trichuris*, and hookworms; Chan, 1997; Renslo and McKerrow, 2006). These numbers will only grow in the future as increased population and urbanization correspond with a rising prevalence of helminth infections (Chan, 1997). Parasitic nematodes also cause considerable losses in livestock and domestic animals, especially in developing nations, and damage a wide range of crops with significant reductions in agricultural production (Witty, 1999; Jasmer et al., 2003). Although current compounds targeting nematode parasites are chemically varied, growing drug resistance drives the need to discover both new biochemical targets and antiparasitic agents. Recent identification of an essential pathway for the biosynthesis of phosphocholine (pCho) in nematodes and *Plasmodium falciparum* (the malaria parasite) that differs from the major phospholipid biosynthesis routes in mammals provides new molecular targets for antiparasitic inhibitor development.

Phosphorylation of choline and its incorporation into phospholipids by the de novo choline or Kennedy pathway supplies the majority of phosphatidylcholine (PtdCho) in mammals, fungi, and some bacteria (Carman and Henry, 1989; Kent, 1995; Lykidis and Jackowski, 2001; Sohlenkamp et al., 2003). Methylation of phosphatidylethanolamine to PtdCho through the Bremer-Greenberg pathway is a second route in humans and yeast (Kent, 1995; Kanipes and Henry, 1997). Plants use a third pathway, not found in mammals, fungi, or bacteria, for the synthesis of choline-derived molecules via the phosphobase methylation pathway (Datko and Mudd, 1988). This pathway involves the methylation of phosphoethanolamine (pEA) to pCho by phosphoethanolamine methyltransferase (PMT; Bolognese and McGraw, 2000; Nuccio et al., 2000; Charron et al., 2002; Mou et al., 2002; Cruz-Ramírez et al., 2004; Figure 1A). The resulting pCho then enters the Kennedy pathway for biogenesis of PtdCho. Recent work examining pCho synthesis in the nematode *Caenorhabditis elegans* and the protozoan malaria parasite *P. falciparum* indicates that these organisms require plant-like PMT for normal growth and development (Pessi et al., 2004; Palavalli et al., 2006; Brendza et al., 2007; Jez, 2007; Lee and Jez, 2011).

Although plants, nematodes, and *Plasmodium* rely on phosphobase methylation for pCho synthesis, the organization of the PMT found in each organism varies (Figures 1B and 1C). Amino acid sequence motifs for S-adenosyl-L-methionine (SAM) binding define the methyltransferase domains in the plant (type I), *Plasmodium* (type II), and nematode (type III) PMT (Kagan and Clarke, 1994). The plant PMTs are di-domain methyltransferases in which the N-terminal domain (MT1) catalyzes the methylation of pEA to phosphomonomethylethanolamine (pMME) and the C-terminal domain (MT2) methylates pMME to phosphodimethylethanolamine (pDME) and pDME to pCho (Bolognese and McGraw, 2000; Nuccio et al., 2000; Charron et al., 2002; Mou et al., 2002; Cruz-Ramírez et al., 2004). The type II PMT from *P. falciparum* (PfPMT) is half the length of the plant enzyme and consists of a single methyltransferase domain that accepts all three phosphobases as substrates (Pessi et al., 2004). In *C. elegans* and other nematodes, two genes encode type III PMT containing either the N-terminal

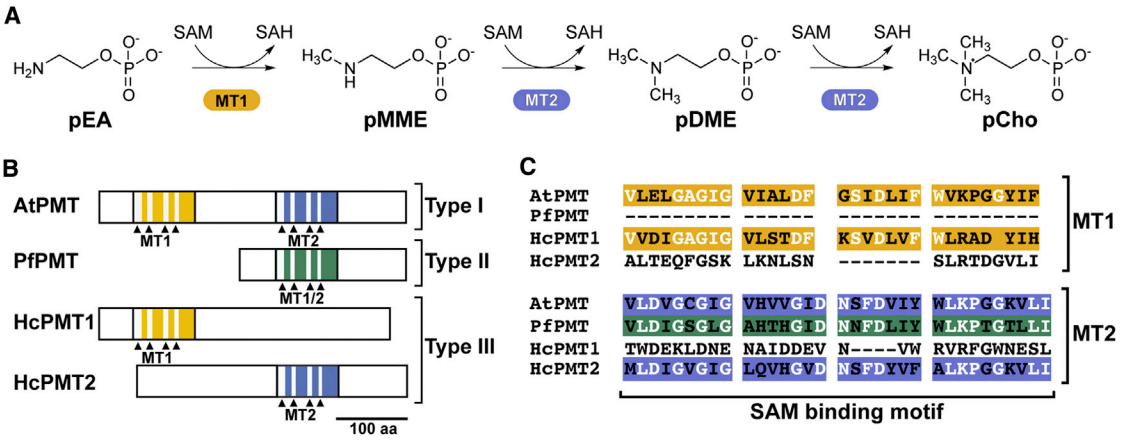

Figure 1. Phosphobase Methylation and the PMT

(A) The phosphobase methylation pathway supplies phosphocholine (pCho) by the sequential methylation of phosphoethanolamine (pEA). The first methyltransferase domain (MT1; gold) catalyzes the conversion of pEA to phosphomonomethylethanolamine (pMME). The second methyltransferase domain (MT2; blue) catalyzes the methylation of pMME to phosphodimethylethanolamine (pDME) and pDME to pCho.

(B) Methyltransferase domain organization of type I (plant), II (*Plasmodium*), and III (nematode) PMT.

(C) Sequence comparison of SAM-binding motifs in the MT1 and MT2 domains of *Arabidopsis thaliana* PMT (AtPMT), *Plasmodium falciparum* PMT (PfPMT), *Haemonchus contortus* PMT1 (HcPMT1), and *H. contortus* PMT2 (HcPMT2).

methyltransferase domain (PMT1) or the C-terminal methyltransferase domain (PMT2; Palavalli et al., 2006; Brendza et al., 2007; Lee et al., 2011). Biochemical studies of the enzymes from *C. elegans* and the parasitic nematode *Haemonchus contortus* (sheep barber pole worm) demonstrate that PMT1 only methylates pEA to pMME and that PMT2 catalyzes the last two reactions in the pathway (Palavalli et al., 2006; Brendza et al., 2007; Lee et al., 2011). Sequence analysis of the plant and nematode PMT suggest a loss of the SAM-binding site in the C-terminal domain of PMT1 and the N-terminal domain of PMT2 (Figures 1B and 1C; Palavalli et al., 2006; Brendza et al., 2007; Jez, 2007; Lee and Jez, 2011; Lee et al., 2011).

Crystal structures of the single-domain PfPMT provided the first views of these enzymes from any species (Lee et al., 2012a, 2012b). PfPMT adopts a canonical SAM-binding fold (Liscombe et al., 2012) with a helical active site "lid-region" forming the phosphobase binding site. Crystallographic and kinetic analyses of PfPMT suggest that ligand binding results in structural rearrangements that bring catalytic residues (i.e., Tyr19 and His132 in PfPMT) into the active site to lock reactants in place for catalysis (Lee et al., 2012a). Although this structure suggests a possible reaction mechanism for the PMT, the active site residues found in PfPMT and the putative catalytic residues in the MT2 domains of the plant and nematode enzymes are missing from the MT1 domains.

The structural and chemical basis for the evolution of the di-domain architecture and phosphobase reaction specificity in the nematode PMT is unclear. Moreover, because the PMTs are not found in mammals and are essential for the normal growth and development of nematodes and *Plasmodium* (Pessi et al., 2004; Palavalli et al., 2006; Brendza et al., 2007), these enzymes are promising targets for antiparasitic inhibitor development. Here, we present the three-dimensional structures of both type III PMTs from *H. contortus*, which reveal the basis for structural modularity in this biosynthetic system, define the mechanistic divergence of their function, and provide insight on the evolution of enzyme function and molecular architecture in the phosphobase methylation pathway of plants, nematodes, and protozoans.

RESULTS

Overall Architectures of Nematode PMT

The X-ray crystal structures of *H. contortus* PMT1 (HcPMT1) in complex with pEA and S-adenosylhomocysteine (SAH) and *H. contortus* PMT2 (HcPMT2) in complex with SAM were both solved using selenomethionine (SeMet)-substituted protein and single-wavelength anomalous dispersion (SAD; Figure 2; Table 1). The structure of the HcPMT2•SAH•pMME complex was determined by molecular replacement. Both enzymes function as monomeric proteins (Lee et al., 2011). The overall structures of HcPMT1 (Figures 2A and 2B) and HcPMT2 (Figures 2C and 2D) reveal di-domain architectures in which a helical linker region connects the N- and C-terminal halves of each molecule. Within each enzyme, the N- and C-terminal domains are structurally distinct, but the functional methyltransferase domains retain the canonical SAM-binding fold comprised of a central seven-stranded β sheet flanked by two α-helical regions (Liscombe et al., 2012). Comparison of the catalytic domains of HcPMT1 and HcPMT2 (Figure 3A) highlights the conservation of the SAM-binding fold across the functional domains and emphasizes the structural differences in the lid region of each domain. For example, in HcPMT1 two α helices (α1 and α2) and the large β5-α10 loop define the phosphobase binding site, whereas the analogous site in HcPMT2 includes two α helices (α9 and α10) along the core β sheet and the α helices of the lid region (α17–19). These structural differences lead to distinct active site architectures in the methyltransferase domains of each enzyme. The crystal structures of HcPMT1 and HcPMT2 also define common

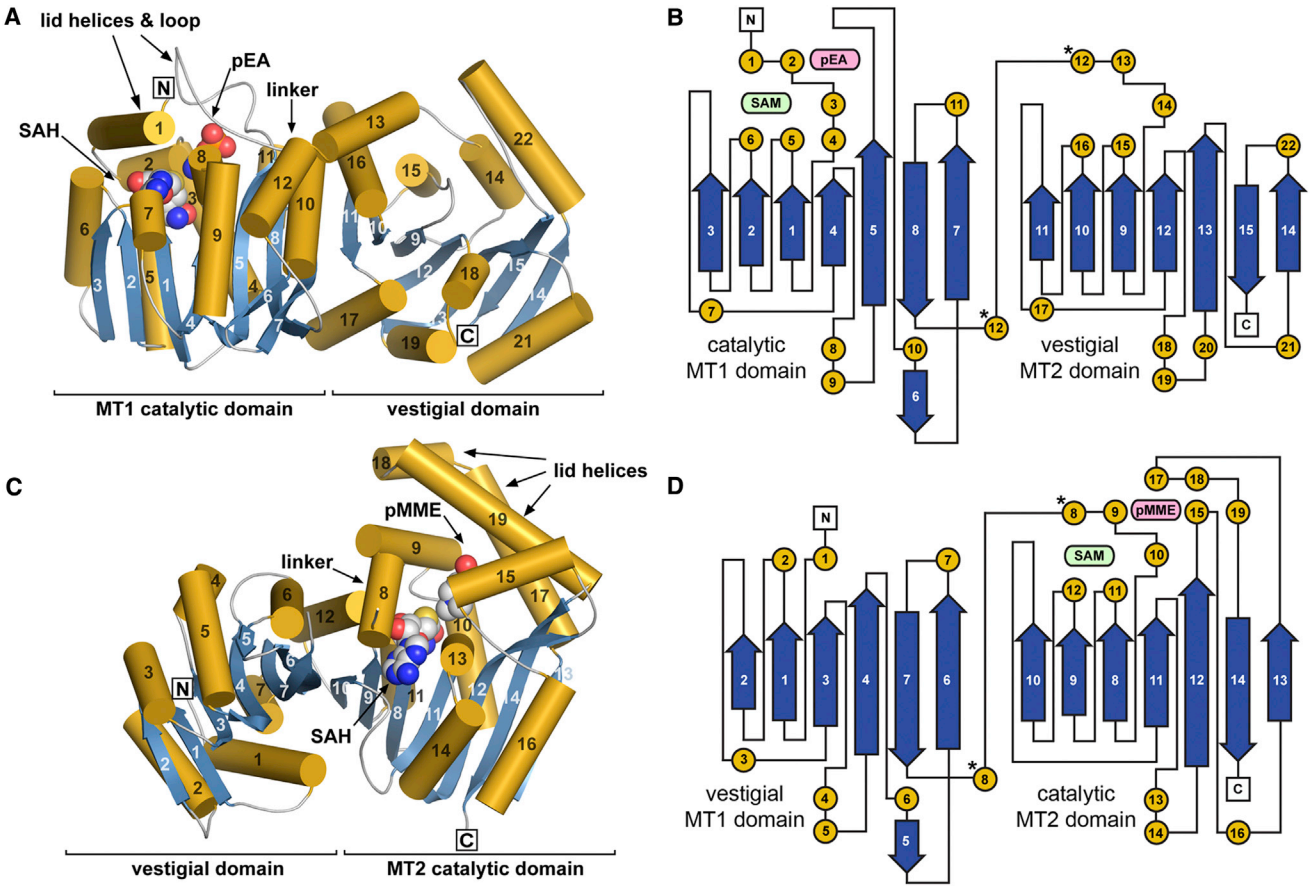

Figure 2. Overall Structures of the Type III PMT

(A) Ribbon diagram of the HcPMT1•SAH• pEA complex with α helices and β strands colored gold cylinders and blue arrows, respectively. Ligands are shown as space-filling models. The catalytic and vestigial methyltransferase domains, as well as the lid region of each functional domain and the linker helices, are indicated.

(B) Topology of HcPMT1 showing the N-terminal MT1 domain and the vestigial C-terminal domain. Regions corresponding to α helices and β strands are gold and blue, respectively. The star indicates the helical linker region.

(C) Ribbon diagram of the HcPMT2•SAH•pMME complex. Coloring of secondary structure and ligand representations are as noted in (A).

(D) Topology of HcPMT2 showing the N-terminal vestigial domain and the C-terminal MT2 domain. Coloring is as in (B).

See also Figure S1.

features in the PMT from a wide variety of nematodes and plants (Figure S1 available online).

Vestigial Domains in Nematode PMT

In the nematode PMT, only one functional methyltransferase domain is located at either the N (HcPMT1) or C terminus (HcPMT2). In each of these enzymes, the other domain is a nonfunctional vestigial domain (Figure 2). The loss of methyltransferase function in each vestigial domain occurs through different structural changes in HcPMT1 and HcPMT2.

The vestigial N-terminal domain of HcPMT2 underwent drastic structural changes compared to the catalytic domain of HcPMT1 (Figures 2B, 2D, and 3B). The HcPMT2 vestigial domain lacks four α helices (α1–4) found around the active site of HcPMT1. In particular, the loss of the two N-terminal α helices in the vestigial domain eliminates the active site "capping" feature observed in HcPMT1. Also, one β strand of the core seven-stranded β sheet is missing. Overall, these major changes effectively eliminate the secondary structure elements that define the active site of HcPMT1.

The loss of activity in the vestigial C-terminal domain of HcPMT1 results from a loop insertion in the location analogous with the SAM/SAH binding site and loss of the α-helical lid-region (Figures 2B, 2D, and 3C). Compared to the three-residue β8–α11 loop in the catalytic domain of HcPMT2, the corresponding loop of the vestigial domain in HcPMT1 (β9–α15) is elongated to 11 residues and fills the space that would form the SAM/SAH binding site. The loss of the lid-region α helices effectively removes the phosphobase site. These structural alterations disrupt the architecture of the substrate binding sites, even though the vestigial domain retains the overall SAM-binding fold topology.

SAM/SAH Binding Site and Movement of the Active Site Lid

Unambiguous electron density for SAM/SAH and phosphobase substrates clearly defines the active sites of HcPMT1 and

Table 1. Summary of Crystallographic Statistics

Crystal	HcPMT1(SeMet)•SAH•pEA	HcPMT2(SeMet)•SAM	HcPMT2•SAH•pMME
Space group	$P6_5$	$I2_3$	C2
Cell dimensions	*a* = *b* = 73.00 Å, *c* = 360.6 Å	*a* = *b* = *c* = 184.5 Å	*a* = 136.0 Å, *b* = 136.8 Å, *c* = 90.87 Å; b = 118.4°
Data Collection			
Wavelength (Å)	0.979	0.979	0.979
Resolution (Å)	36.5–1.68 (1.73–1.68)	41.3–3.00 (3.05–3.00)	34.2–1.72 (1.75–1.72)
Reflections (total/unique)	1,126,179/118,485	110,297/21,029	564,292/150,732
Completeness (%)	100 (100)	99.7 (99.4)	98.2 (97.6)
$\langle I/\sigma \rangle$	35.4 (3.0)	32.9 (2.7)	30.4 (2.1)
R_{sym} (%)	7.2 (67.7)	9.4 (58.2)	7.3 (68.1)
Refinement			
R_{cryst}/R_{free}	12.2/14.0	23.9/28.6	17.5/21.0
No. of protein atoms	7,653	6,932	10,342
No. of water molecules	2,035	0	1,006
No. of ligand atoms	98	54	150
Rmsd, bond lengths (Å)	0.005	0.006	0.006
Rmsd, bond angles (°)	0.098	1.011	1.036
Ave. B-factor (Å^2), prot, water, ligand	24.1, 39.3, 39.8	68.7, –, 121	37.0, 45.6, 30.3
Stereochemistry: favored, allowed, outlier (%)	97.3, 2.7, 0.0	98.5, 1.5, 0.0	98.2, 1.6, 0.2

Numbers in parentheses represent highest-resolution shell.

HcPMT2 (Figure S2). The SAM/SAH binding site is situated along the N-terminal face of the core seven-stranded β sheet structure (Figure 2) with conserved residues in the SAM-binding motif generally located in the β strands of the core fold (Figure S1). The general architecture of the SAM/SAH binding site in each PMT includes a network of negatively charged side chains, water-mediated contacts, and backbone atoms of conserved amino acid residues (Figure 4). In each structure, multiple apolar residues sandwich the adenine ring of SAM/SAH and an invariant aspartate interacts with the ribose hydroxyl groups. For example, Asp80 in HcPMT1 and Asp250 in HcPMT2 form a bridging contact with the hydroxyl groups of the ribose moiety of SAH. In addition to the hydrogen bond network, extensive van der Waals contacts with multiple aromatic and apolar amino acid residues are associated with SAM/SAH binding in both structures; however, unlike the hydrogen bond network, the residues for hydrophobic interactions are not well conserved between these domains. Previous thermodynamic analysis of SAH binding to the nematode enzymes suggested a larger nonpolar interaction surface in HcPMT1 compared to HcPMT2 (Lee et al., 2011), which is corroborated by the crystal structures. The SAM/SAH binding site of HcPMT1 contains multiple aromatic residues (Trp14, Phe65, Phe81, and Trp123) that provide favorable van der Waals interactions that lead to tighter affinity of HcPMT1 for SAM and SAH versus HcPMT2.

The HcPMT structures also imply movement of the lid-domain and the helical linker region to cover the active site for catalysis (Figures 4A and 4B). In both structures, the active sites are capped by secondary structure elements. In HcPMT1, three N-terminal α helices (α2, α3, and α4) enclose the SAM/SAH binding site. Likewise, the helical linker region (α8 and α9) of HcPMT2 forms part of the lid-region that locks ligands in the active site and contributes the catalytic tyrosine into the active site, as described later. Thus, the catalytic domains of HcPMT1 and HcPMT2 have solvent inaccessible active sites when both SAM/SAH and phosphobase substrates are bound.

Phosphobase Selectivity

The phosphobase binding sites of HcPMT1 and HcPMT2 are structurally distinct (Figures 5A and 5B). In HcPMT1, an extensive hydrogen bond network and multiple van der Waals contacts lock pEA in the active site (Figure 5A). The backbone nitrogen of Ser160, the N_ε of His170, and the hydroxyl groups of Ser155, Ser160, and Tyr180 interact with the substrate phosphate group. Three conserved threonines (Thr161, Thr168, and Thr178) also mediate water interactions with the phosphate group. Met26, Met27, Leu28, Trp123, and Pro159 contribute additional surface contacts. The phosphobase binding site of HcPMT2 is nearly identical to that of PfPMT (Lee et al., 2012a) and contains a cluster of tyrosines and basic residues (Figures 5B and 5C). The hydroxyl groups of Tyr191, Tyr325, Tyr339, and Tyr345 hydrogen bond to the phosphate group of pMME (Figure 5B). Charge-charge interactions between the phosphate and the side chains of Arg373 and Lys411 also contribute to binding.

Comparison of the active sites in HcPMT1 and HcPMT2 reveals the structural basis for phosphobase specificity of each enzyme. In HcPMT1, Trp14, Met26, Met27, and Trp123 constrict the space between the SAM/SAH and phosphobase binding sites (Figures 5D and 5G). Tyr127 hydrogen bonds with the

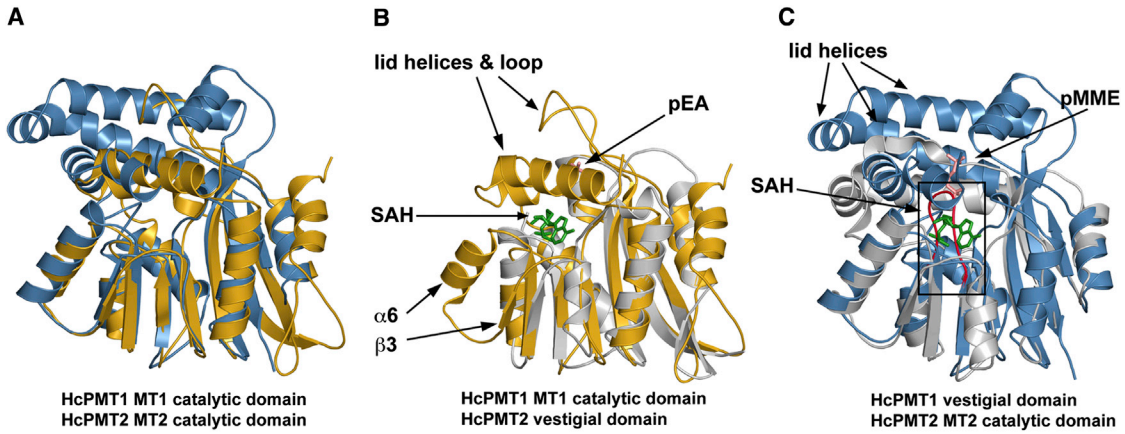

Figure 3. Comparison of Catalytic Domains and Vestigial Domains of Nematode PMT

(A) Superimposition of the catalytic domains of HcPMT1 (gold) and HcPMT2 (blue).

(B) Structural comparison of the MT1 domain of HcPMT1 (gold) and the vestigial N-terminal domain of HcPMT2 (gray). Major structural differences are indicated with arrows.

(C) Structural comparison of the MT2 domain of HcPMT2 (blue) and vestigial C-terminal domain of HcPMT1 (gray). The box indicates the region of the elongated loop (red) in the vestigial domain and the arrows highlight structural differences in the lid region.

amine of pEA and orients the lone pair toward the SAM/SAH site for the ensuing methylation reaction. A different collection of active site residues in HcPMT2 alters the shape of the interface between the substrate binding sites. In HcPMT2, the positioning of Tyr183 and His295 widen the space around pMME to readily accommodate the larger pDME and pCho molecules (Figures 5E and 5H). A similar architecture is also seen in PfPMT (Figures 5F and 5I).

Modeling of SAM into the HcPMT1•SAH•pEA and HcPMT2•SAH•pMME structures provides insight on how the steric gating of methylation substrates occurs between the MT1 and MT2 active sites. In HcPMT1, the S_{δ}-C_{ε} of SAM and the nitrogen of pEA are aligned within 2.0 Å of each other, which allows for facile methyl group transfer (Figure 5D). Methylation of pEA to pMME is readily accommodated within the narrow active site of HcPMT1; however, additional methylations result in steric clashes with residues surrounding the substrate amine. In contrast, the wider interface of the HcPMT2 active site readily accommodates methylated phosphobases. The positioning of substrates in the HcPMT2 and PfPMT (Figures 5E and 5F) emphasizes how their phosphobase sites contain sufficient space for pDME and pCho.

The structures of the nematode PMT reveal the basis for selective methylation in these enzymes; however, the features that allow PfPMT to methylate all three phosphobase substrates in one active site are unclear. Although the active sites of HcPMT2 (Figures 5B and 5E) and PfPMT (Figures 5C and 5F) are nearly identical, two subtle changes alter water-mediated interactions with pEA and may account for functional differences. In the PfPMT•SAH•pEA complex (Lee et al., 2012a), two water

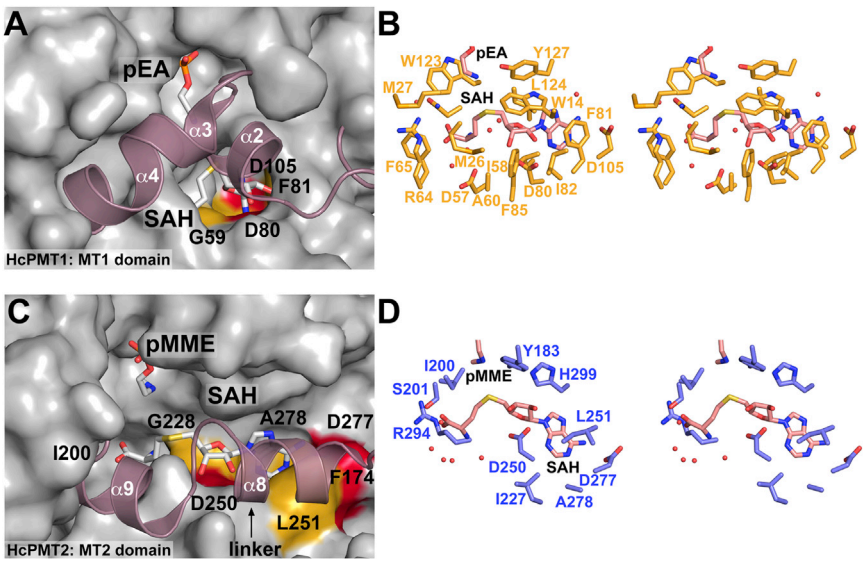

Figure 4. Overall of the SAM/SAH Binding Sites and Active Site Capping

(A and B) The active sites of HcPMT1 (A) and HcPMT2 (B) are shown as surface renderings. Surfaces for invariant Asp residues and other conserved residues in the binding site are highlighted in red and gold, respectively. The helices enclosing the active sites are shown as ribbons (rose).

(C and D) Residues of the SAM/SAH binding site in HcPMT1 (C) and HcPMT2 (D) are shown in stereo view.

See also Figure S2.

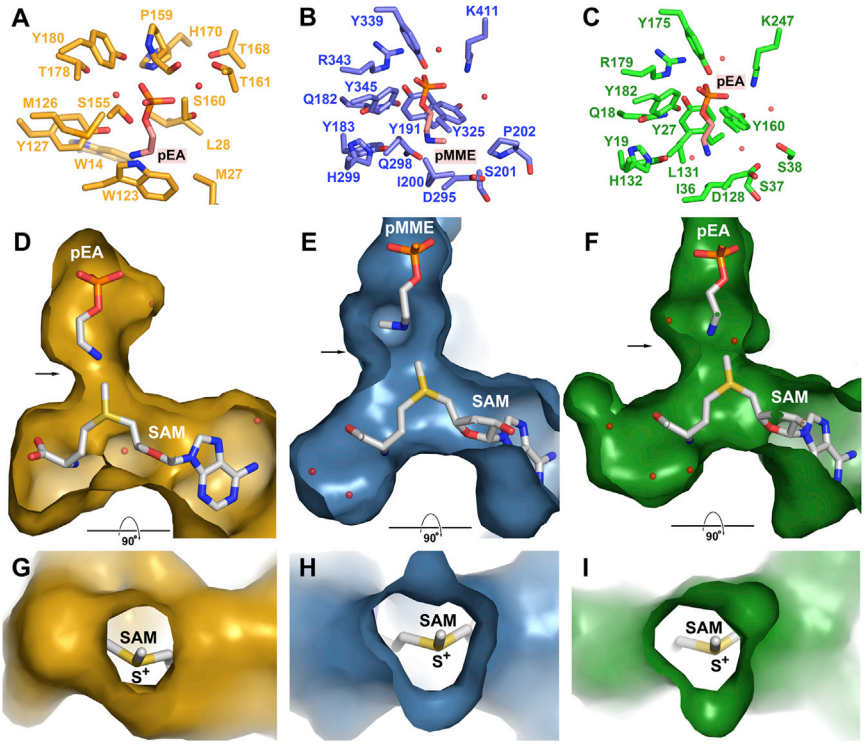

Figure 5. Phosphobase Binding Site and the Molecular Basis for Substrate Specificity

(A–C) Amino acid residues forming interactions with pEA or pMME in HcPMT1 (A), HcPMT2 (B), and PfPMT (C) are shown as stick models and are gold, blue, and green, respectively.

(D–F) Waters forming hydrogen bonds with the ligands are shown as red spheres. The surfaces of the active sites in HcPMT1 (D), HcPMT2 (E), and PfPMT (F) are shown as cut-away views.

(G–I) The arrow indicates the plane used for viewing the opening at the interface between the SAM/SAH and phosphobase sites in HcPMT1 (G), HcPMT2 (H), and PfPMT (I).

molecules are bound near the amine group of pEA and occupy space where the methyl groups of pCho would be situated (Figure 5F). The positioning of each water molecule allows for bridging contacts between the nitrogen of pEA and surrounding residues. These interactions may guide the lone pair of the nitrogen of pEA toward the methyl carbon of SAM for catalysis in PfPMT. In HcPMT2, the presence of Gln298 instead of Leu131 in PfPMT slightly reduces the space around the amine to occlude one water molecule from the site. In PfPMT, a second water molecule interacts with Ser38, but the corresponding residue in HcPMT2 is Pro202, which reduces the size of the binding pocket. These changes in HcPMT2 may disrupt the water-mediated interactions with pEA observed in PfPMT and alter reaction specificity.

To test the potential role of these residues for pEA specificity in the *Plasmodium* enzyme, three PfPMT mutants (S38P, L131Q, and S38P/L131Q) were generated, expressed, purified, and assayed using pEA and pDME as substrates for comparison with wild-type enzyme (Figure 6). Previous analysis of wild-type PfPMT showed comparable catalytic efficiencies with pEA and pDME as substrates (Lee et al., 2012a). Activity assays showed that the S38P mutation abrogated activity with pEA and slightly altered activity with pDME by 2-fold. The L131Q mutant did not significantly change activity with either pEA or pDME. The S38P/L131Q mutant mirrored the effects of the S38P mutation to yield a protein lacking activity with pEA and retaining activity with pDME.

Structurally Distinct Active Sites

Structural and functional studies of PfPMT led to a proposed mechanism that involves general acid/base catalysis (Lee et al., 2012a). In this reaction, nucleophilic attack on the SAM methyl group requires deprotonation of the substrate amine. Intriguingly, the structure of HcPMT1 reveals a strikingly different active site configuration for phosphobase methylation compared to PfPMT and HcPMT2. As noted previously, the binding site of pEA in HcPMT1 completely differs from the phosphobase sites of PfPMT and HcPMT2 and lacks the catalytic dyad observed in PfPMT.

In HcPMT1, the hydroxyl group of Tyr127, which is invariant in the MT1 domains of plant and nematode PMT (Figure S1) is located ~3.5 Å from the methyl group of SAM modeled in the active site and also forms a hydrogen bond with the nitrogen of pEA (2.8 Å) and an adjacent water molecule (2.7 Å) (Figure 7A). The water molecule forms additional contacts with the side-chain hydroxyl of Thr178 (2.9 Å) and the phosphate group of pEA (2.7 Å). His170 interacts with the substrate phosphate

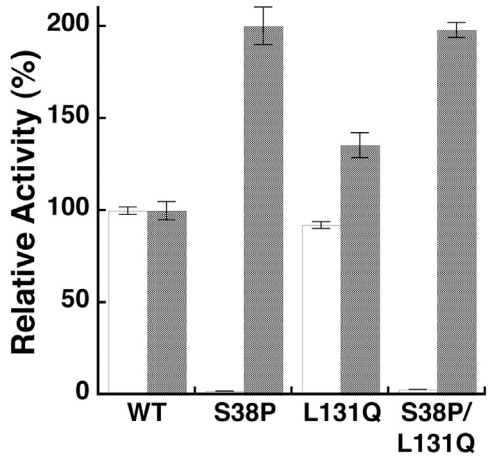

Figure 6. Phosphobase Selectivity

A comparison of the relative specific activities of wild-type (WT), S38P, L131Q, and S38P/L131Q PfPMT using pEA (white bars) and pDME (gray bars) as substrates is shown.

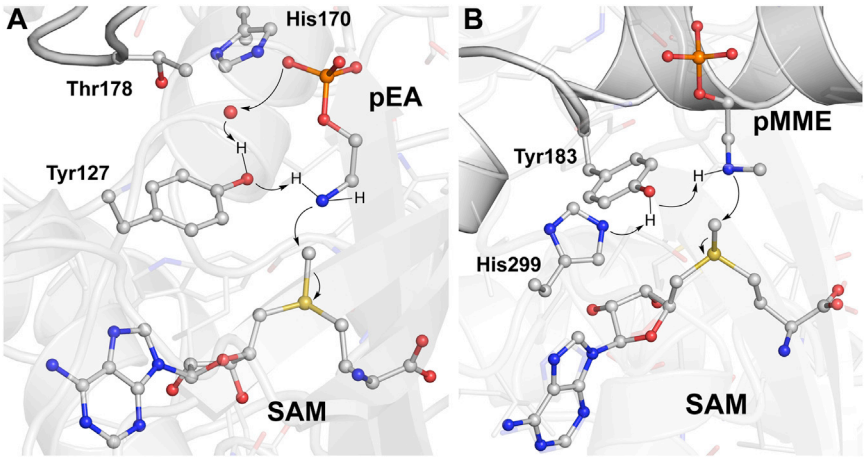

Figure 7. Two Distinct Reactions for Phosphobase Methylation
The putative catalytic residues of HcPMT1 (A) and HcPMT2 (B) are shown. The proposed roles of Tyr127 in HcPMT1 and the Tyr183-His299 dyad in HcPMT2 are indicated.

(2.7 Å). The positioning of Tyr127 suggests a potential catalytic role in the methylation of pEA to pMME.

The HcPMT2 structure reveals a tyrosine-histidine dyad poised for catalysis, as observed in PfPMT (Lee et al., 2012a). The hydroxyl group of Tyr183 (equivalent to Tyr19 in PfPMT) is positioned between the N_1 of pMME (3.7 Å) and methyl group of modeled SAM (3.0 Å) (Figure 7B). The N_ε of His299 (equivalent to His132 in PfPMT) is 2.8 Å away from the tyrosine hydroxyl group and is placed to function as a general base to activate the tyrosine for catalysis.

To examine the catalytic roles of the tyrosines in the MT1 and MT2 active sites, a series of site-directed mutants (HcPMT1: Y127A and Y127F; HcPMT2: Y183A and Y183F) were generated. Previous kinetic analysis of HcPMT1 and HcPMT2 showed these enzymes to be specific for pEA and pMME/pDME, respectively (Lee et al., 2011). Mutation of the critical tyrosine in either HcPMT1 or HcPMT2 significantly disrupts enzymatic activity. Substitution of an alanine for either residue yields mutant proteins with no detectable activity; however, the HcPMT1 Y127F mutant retained 3% of wild-type activity with pEA (17.6 ± 3.3 versus 550 ± 12 nmol min^{-1} mg $protein^{-1}$) and the HcPMT2 Y183F mutant displayed 5% of wild-type activity with pDME (15.6 ± 0.6 versus 312 ± 7 nmol min^{-1} mg $protein^{-1}$).

DISCUSSION

The adaptability of protein structure provides a foundation for the rapid evolution of metabolic modularity and molecular diversity across biochemical pathways (Peregrín-Alvarez et al., 2009; Caetano-Anollés et al., 2009; Liscombe et al., 2012). The crystal structures of the di-domain PMT from the nematode *H. contortus*, along with the multifunctional PfPMT, reveal the varied architectural and mechanistic solutions used in these organisms to supply pCho for membrane biogenesis. Although the overall architecture of the PMT from nematodes and *Plasmodium* varies (Figure 1), the core methyltransferase fold provides a versatile platform for remodeling of the structural features necessary for substrate and reaction specificity in the nematode PMT (Figure 2).

The structural features of the lid region in HcPMT1 provide an active site that is highly specific for pEA (Figure 2). The steric constraints of the interface between the phosphobase and SAM/SAH binding sites suggest a molecular basis for the selectivity of methylating pEA to pMME, because the physical size of the active site effectively prevents the accommodation of pDME and pCho as substrates (Figures 5A, 5D, and 5G), whereas the wider interface of the HcPMT2 active site readily allows for conversion of pMME to pDME and pDME to pCho (Figures 5B, 5E, and 5H). In this case, the basis for selectivity against pEA methylation may result from conformational flexibility with the amine group of pEA sampling alternate binding modes when bound at the MT2 active site. The inhibitory effect of pEA versus pMME and pDME substrates in HcPMT2 suggests this is the case (Lee et al., 2011). The addition of methyl groups at the amine moiety of the phosphobases may provide van der Waals contacts that constrain movement of this moiety to position it near SAM for efficient catalysis.

Comparison of the HcPMT2 (Figures 5B and 5E) and PfPMT (Figures 5C and 5F) crystal structures suggests that subtle active site differences can also influence phosphobase selectivity. Pro202 and Gln298 in HcPMT2 replace Ser38 and Leu131 in PfPMT. In PfPMT, these differences provide space near the nitrogen of pEA for water-mediated contacts that may orient this substrate for catalysis. In HcPMT2, the larger amino acids slightly constrict the space at the interface, which may disrupt the water-mediated interactions to alter reaction specificity. Functional analysis of site-directed mutants of PfPMT shows that substitution of Ser38 with a proline is sufficient to cause a loss of activity with pEA, with modest changes in activity with pDME (Figure 6). In contrast, substitution of Leu131 in PfPMT has little effect on phosphobase selectivity (Figure 6). Thus, the S38P mutation appears critical for altering phosphobase selectivity in PfPMT.

The nematode PMT1 and PMT2 also use different active site configurations for phosphobase methylation (Figure 7). Although the active sites of each domain maintain the overall positioning of phosphobase and SAM substrates, the residues required for deprotonation of the substrate amine and nucleophile alignment differ in each protein.

The overall reactions catalyzed by the MT1 and MT2 active sites are similar, but use different active site architectures for deprotonation of the phosphobase amine. In HcPMT1, Tyr127 is positioned to hydrogen bond with the amine group of pEA and an adjacent water molecule interacts with Thr183 and the substrate phosphate group (Figure 7A). Analysis of the HcPMT1 Y127F mutant indicates a critical role for this residue in catalysis. Based on the crystal structure, a possible mechanism involving substrate-assisted catalysis for deprotonation of pEA is

proposed (Dall'Acqua and Carter, 2000; Wang et al., 2007). The positioning of the substrate phosphate group relative to the water molecule bound by Tyr127 and Thr178 suggests a possible proton relay. For pEA methylation, the hydroxyl proton of Tyr127 is relayed via the water molecule to the phosphate group of pEA. This activates the hydroxyl group of Tyr127 to deprotonate the amine for methyl group transfer from SAM.

In contrast, the HcPMT2 active site contains the tyrosine-histidine dyad originally observed in PfPMT (Lee et al., 2012a; Figure 7B). The identical active sites of HcPMT2 and PfPMT imply a conserved chemical mechanism for these enzymes. Extensive structural and functional analyses of PfPMT suggest that the histidine residue serves as a general base to abstract a proton from the tyrosine hydroxyl group to activate it for catalysis and deprotonation of the alkylamine (Figure 7B). Mutagenesis of Tyr183 in HcPMT2 results in a loss of methyltransferase activity.

Although the MT1 and MT2 active sites use different architectures for catalysis, both also share common features. Each active site places the reactive groups of SAM and phosphobases in proximity and excludes solvent from the site to allow for transmethylation (Zubieta et al., 2003; Liscombe et al., 2012). In each active site, a critical tyrosine orients the reactive amine toward the methyl group of SAM. The structural and chemical variation in the HcPMT1 and HcPMT2 active sites also suggests different reaction energies that may reflect the reactivity of the various phosphobase substrates.

The structural organization of the PMT from plants, nematodes, and *Plasmodium* likely derives from evolutionary history and the varied demand for pCho in these diverse organisms. Evolutionarily, the PMT likely appeared first in the plant lineage as the bifunctional type I enzyme. In plants, the PMT provide pCho for the production of the osmotic protectant glycine betaine and of phospholipid membranes (Datko and Mudd, 1988; Kanipes and Henry, 1997; Bolognese and McGraw, 2000; Nuccio et al., 2000; Charron et al., 2002; Mou et al., 2002; Cruz-Ramírez et al., 2004). Biochemical regulation of the plant PMT by feedback inhibition and transcriptional changes (i.e., induction by salt stress and repression by choline) play major roles in controlling flux through the pathway (Weretilnyk et al., 1995; Kanipes and Henry, 1997; Nuccio et al., 1998). Expression of a single bifunctional PMT in plants allows for dedicated coordination of pathway flux in response to environmental stresses and physiologic changes.

Nematodes, as a phylum, evolved 600–1,200 million years ago and fill a wide range of ecologic and physiologic niches (Blaxter, 1998). Gene duplication of a plant-like PMT followed by loss of function in the vestigial domains led to specialized type III PMT in the nematode lineage. It is likely that this divergence and specialization of biochemical function occurred early on because the evolution of nematode clades is ancient and maintained by a strong evolutionary pressure as distinct PMT1 and PMT2 are highly conserved in the genomes of free-living and parasitic nematodes (Palavalli et al., 2006; Brendza et al., 2007; Jez, 2007). Although both PMT1 and PMT2 are essential for normal growth and development of *C. elegans* (Palavalli et al., 2006; Brendza et al., 2007), recent studies implicate PMT1 as part of a metabolic control circuit that maintains cholesterol and lipid homeostasis (Li et al., 2011; Walker et al., 2011). In *C. elegans*, levels of PtdCho and/or SAM alter maturation of sterol regulatory element-binding proteins (SREBPs) to control expression of genes related to one-carbon metabolism, including CePMT1. As a free-living soil organism, regulation of lipid homeostasis in *C. elegans* is likely critical to respond to changing nutrient and feeding conditions (Brooks et al., 2009; Mullaney and Ashrafi, 2009; Watts, 2009). To date, a similar regulatory circuit has not been identified in either plants or *Plasmodium*. The divergence of PMT function in nematodes appears to allow for metabolic control at the initial reaction step in the phosphobase pathway.

Plasmodium are protozoan parasites of humans; however, the evolutionary origin of all apicomplexans begins with an ancient photosynthetic ancestor (Fast et al., 2001). The conserved structure and sequence of PfPMT suggests that evolution of the single-domain type II enzyme is also ancient, but either lost or maintained in various protozoa depending on host environment and possible source of phospholipid precursors (Pessi et al., 2004, Lee and Jez, 2011). Regulation of the *Plasmodium* enzyme has not been well studied, but the role of PfPMT in peak membrane biogenesis at the trophozoite stage likely places high demand on the pathway (Pessi et al., 2004).

In addition to providing snapshots of the diverse structural and functional evolution of a critical biochemical pathway in across nematodes, plants, and *Plasmodium*, the structures of the PMT provide a template for the development of inhibitors targeting parasites of humans and animals that rely on the phosphobase methylation pathway for membrane biogenesis. Because the PMTs are not found in mammals and are required for normal growth of nematodes and *Plasmodium*, these enzymes are candidates for antiparasitic drug discovery efforts. Moreover, the structural differences between the active sites provide distinct molecular targets for the development of small molecule inhibitors of these proteins.

EXPERIMENTAL PROCEDURES

Cloning and Mutagenesis

The pET-28a-HcPMT1, pET-28a-HcPMT2, and pET-28a-PfPMT constructs were previously described (Lee et al., 2011, 2012b). Site-directed mutants were generated using the QuikChange PCR method (Agilent Technologies).

Protein Expression and Purification

Wild-type and mutant enzymes were expressed as N-terminal His-tag fusion proteins in *Escherichia coli* Rosetta II (DE3) cells (EMD Millipore) and were purified using nickel-affinity and size-exclusion chromatographies, as previously described (Palavalli et al., 2006; Brendza et al., 2007; Lee et al., 2011, 2012a). Thrombin digestion was used to remove the N-terminal His-tag prior to crystallization. Protein concentrations were determined by the Bradford method (Bio-Rad) with bovine serum albumin as standard. SeMet-substituted proteins were produced by inhibition of the *E. coli* methionine biosynthesis pathway with the same vector and bacterial strain used for native protein expression (Van Duyne et al., 1993). Incorporation of SeMet was confirmed by electrospray ionization mass spectrometry to compare intact molecular masses of native and derivatized protein. Purification of SeMet-substituted proteins used the same protocol as native protein.

Protein Crystallography

All protein crystals were grown by the hanging drop vapor diffusion method at 4°C. Crystals of SeMet-substituted HcPMT1 (15 mg/ml) in complex with SAH (0.5 mM) and pEA (5 mM) formed in drops of a 1:1 mixture of protein

and crystallization buffer (0.2 M lithium sulfate monohydrate, 0.1 M Tris·HCl [pH 8.5], 30% PEG-4,000, and 0.5% n-octyl-β-D-glucoside). Crystals of SeMet-substituted HcPMT2 (12.0 mg/ml) in complex with SAM (5 mM) grew in drops of a 2:1 mixture of protein and crystallization buffer (0.1 M Tris·HCl [pH 9.0] and 25% PEG-400). Crystals of native HcPMT2 (12 mg/ml) in complex with SAH (0.5 mM) and pMME (5 mM) were grown in drops of a 1:1 mixture of protein and crystallization buffer (0.1 M sodium citrate [pH 5.0], 20% PEG-3,000). All crystals were stabilized in cryoprotectant (crystallization solution with 30% glycerol) before flash freezing in liquid nitrogen for data collection at 100 K. The HcPMT1 and HcPMT2 structures were solved by SAD phasing. All diffraction data were collected at beamline 19ID of the Argonne National Lab Advanced Photon Source and used HKL3000 (Minor et al., 2006) to index, integrate, and scale the data sets. For SAD phasing, SHELX (Sheldrick, 2008) was used to determine initial SeMet positions and to estimate initial phases from the peak wavelength data set. Refinement of SeMet positions and parameters was performed with MLPHARE (CCP4, 1994). Solvent flattening used DM (Terwilliger, 2000) with ARP/wARP (Morris et al., 2003) to build an initial model. COOT (Emsley and Cowtan, 2004) and PHENIX (Adams et al., 2010) were used for iterative rounds of manual model building and refinement, respectively. The structure of the HcPMT2·SAH·pMME complex was solved by molecular replacement in PHASER (McCoy et al., 2007) using the SeMet-substituted HcPMT2 structure as a search model. Data collection and refinement statistics are summarized in Table 1.

Enzyme Assays

Assays of PMT activity were performed using a previously described radiochemical assay (Palavalli et al., 2006; Brendza et al., 2007, Lee et al., 2012b). Protein amount and time of reaction provided a linear rate of product formation.

ACCESSION NUMBERS

The Protein Data Bank accession numbers for the atomic coordinates and structure factors reported in this paper are 4KRG (for HcPMT1·SAH·pEA), 4KRH (for HcPMT2·SAM), and 4KRI (for HcPMT2·SAH·pMME).

SUPPLEMENTAL INFORMATION

Supplemental Information includes two figures and can be found with this article online at http://dx.doi.org/10.1016/j.str.2013.07.023.

ACKNOWLEDGMENTS

This work was supported by a grant from the National Institutes of Health (AI-097119). Portions of this research were carried out at the Argonne National Laboratory Structural Biology Center of the Advanced Photon Source, a national user facility operated by the University of Chicago for the Department of Energy Office of Biological and Environmental Research (DE-AC02-06CH11357).

Received: June 17, 2013
Revised: July 25, 2013
Accepted: July 28, 2013
Published: September 5, 2013

REFERENCES

Adams, P.D., Afonine, P.V., Bunkóczi, G., Chen, V.B., Davis, I.W., Echols, N., Headd, J.J., Hung, L.W., Kapral, G.J., Grosse-Kunstleve, R.W., et al. (2010). PHENIX: a comprehensive Python-based system for macromolecular structure solution. Acta Crystallogr. D Biol. Crystallogr. *66*, 213–221.

Blaxter, M.L. (1998). *Caenorhabditis elegans* is a nematode. Science *282*, 2041–2046.

Bolognese, C.P., and McGraw, P. (2000). The isolation and characterization in yeast of a gene for Arabidopsis S-adenosylmethionine:phospho-ethanolamine N-methyltransferase. Plant Physiol. *124*, 1800–1813.

Brendza, K.M., Haakenson, W., Cahoon, R.E., Hicks, L.M., Palavalli, L.H., Chiapelli, B.J., McLaird, M., McCarter, J.P., Williams, D.J., Hresko, M.C., and Jez, J.M. (2007). Phosphoethanolamine N-methyltransferase (PMT-1) catalyses the first reaction of a new pathway for phosphocholine biosynthesis in Caenorhabditis elegans. Biochem. J. *404*, 439–448.

Brooks, K.K., Liang, B., and Watts, J.L. (2009). The influence of bacterial diet on fat storage in *C. elegans*. PLoS ONE *4*, e7545.

Caetano-Anollés, G., Wang, M., Caetano-Anollés, D., and Mittenthal, J.E. (2009). The origin, evolution and structure of the protein world. Biochem. J. *417*, 621–637.

Carman, G.M., and Henry, S.A. (1989). Phospholipid biosynthesis in yeast. Annu. Rev. Biochem. *58*, 635–669.

CCP4 (Collaborative Computational Project, Number 4). (1994). The CCP4 suite: programs for protein crystallography. Acta Crystallogr. D Biol. Crystallogr. *50*, 760–763.

Chan, M.S. (1997). The global burden of intestinal nematode infections—fifty years on. Parasitol. Today (Regul. Ed.) *13*, 438–443.

Charron, J.B., Breton, G., Danyluk, J., Muzac, I., Ibrahim, R.K., and Sarhan, F. (2002). Molecular and biochemical characterization of a cold-regulated phosphoethanolamine N-methyltransferase from wheat. Plant Physiol. *129*, 363–373.

Cruz-Ramírez, A., Lóópez-Bucio, J., Ramírez-Pimentel, G., Zurita-Silva, A., Sánchez-Calderon, L., Ramírez-Chávez, E., González-Ortega, E., and Herrera-Estrella, L. (2004). The xipotl mutant of Arabidopsis reveals a critical role for phospholipid metabolism in root system development and epidermal cell integrity. Plant Cell *16*, 2020–2034.

Dall'Acqua, W., and Carter, P. (2000). Substrate-assisted catalysis: molecular basis and biological significance. Protein Sci. *9*, 1–9.

Datko, A.H., and Mudd, S.H. (1988). Enzymes of phosphatidylcholine synthesis in lemna, soybean, and carrot. Plant Physiol. *88*, 1338–1348.

Emsley, P., and Cowtan, K. (2004). Coot: model-building tools for molecular graphics. Acta Crystallogr. D Biol. Crystallogr. *60*, 2126–2132.

Fast, N.M., Kissinger, J.C., Roos, D.S., and Keeling, P.J. (2001). Nuclear-encoded, plastid-targeted genes suggest a single common origin for apicomplexan and dinoflagellate plastids. Mol. Biol. Evol. *18*, 418–426.

Jasmer, D.P., Goverse, A., and Smant, G. (2003). Parasitic nematode interactions with mammals and plants. Annu. Rev. Phytopathol. *41*, 245–270.

Jez, J.M. (2007). Phosphatidylcholine biosynthesis as a potential target for inhibition of metabolism in parasitic nematodes. Curr Enz Inhib *3*, 133–142.

Kagan, R.M., and Clarke, S. (1994). Widespread occurrence of three sequence motifs in diverse S-adenosylmethionine-dependent methyltransferases suggests a common structure for these enzymes. Arch. Biochem. Biophys. *310*, 417–427.

Kanipes, M.I., and Henry, S.A. (1997). The phospholipid methyltransferases in yeast. Biochim. Biophys. Acta *1348*, 134–141.

Kent, C. (1995). Eukaryotic phospholipid biosynthesis. Annu. Rev. Biochem. *64*, 315–343.

Lee, S.G., and Jez, J.M. (2011). The phosphobase methylation pathway in *Caernorhabditis elegans*: a new route to phospholipids in animals. Curr Chem Biol *5*, 183–188.

Lee, S.G., Haakenson, W., McCarter, J.P., Williams, D.J., Hresko, M.C., and Jez, J.M. (2011). Thermodynamic evaluation of ligand binding in the plant-like phosphoethanolamine methyltransferases of the parasitic nematode *Haemonchus contortus*. J. Biol. Chem. *286*, 38060–38068.

Lee, S.G., Kim, Y.C., Alpert, T.D., Nagata, A., and Jez, J.M. (2012a). Structure and reaction mechanism of phosphoethanolamine methyltransferase from the malaria parasite Plasmodium falciparum: an antiparasitic drug target. J. Biol. Chem. *287*, 1426–1434.

Lee, S.G., Alpert, T.D., and Jez, J.M. (2012b). Crystal structure of phosphoethanolamine methyltransferase from *Plasmodium falciparum* in complex with amodiaquine. Bioorg. Med. Chem. Lett. *22*, 4990–4993.

Li, Y., Na, K., Lee, H.J., Lee, E.Y., and Paik, Y.K. (2011). Contribution of *sams-1* and *pmt-1* to lipid homoeostasis in adult *Caenorhabditis elegans*. J. Biochem. *149*, 529–538.

Liscombe, D.K., Louie, G.V., and Noel, J.P. (2012). Architectures, mechanisms and molecular evolution of natural product methyltransferases. Nat. Prod. Rep. *29*, 1238–1250.

Lykidis, A., and Jackowski, S. (2001). Regulation of mammalian cell membrane biosynthesis. Prog. Nucleic Acid Res. Mol. Biol. *65*, 361–393.

McCoy, A.J., Grosse-Kunstleve, R.W., Adams, P.D., Winn, M.D., Storoni, L.C., and Read, R.J. (2007). Phaser crystallographic software. J. Appl. Cryst. *40*, 658–674.

Minor, W., Cymborowski, M., Otwinowski, Z., and Chruszcz, M. (2006). HKL-3000: the integration of data reduction and structure solution—from diffraction images to an initial model in minutes. Acta Crystallogr. D Biol. Crystallogr. *62*, 859–866.

Morris, R.J., Perrakis, A., and Lamzin, V.S. (2003). ARP/wARP and automatic interpretation of protein electron density maps. Methods Enzymol. *374*, 229–244.

Mou, Z., Wang, X., Fu, Z., Dai, Y., Han, C., Ouyang, J., Bao, F., Hu, Y., and Li, J. (2002). Silencing of phosphoethanolamine N-methyltransferase results in temperature-sensitive male sterility and salt hypersensitivity in Arabidopsis. Plant Cell *14*, 2031–2043.

Mullaney, B.C., and Ashrafi, K. (2009). C. elegans fat storage and metabolic regulation. Biochim. Biophys. Acta *1791*, 474–478.

Nuccio, M.L., Russell, B.L., Nolte, K.D., Rathinasabapathi, B., Gage, D.A., and Hanson, A.D. (1998). The endogenous choline supply limits glycine betaine synthesis in transgenic tobacco expressing choline monooxygenase. Plant J. *16*, 487–496.

Nuccio, M.L., Ziemak, M.J., Henry, S.A., Weretilnyk, E.A., and Hanson, A.D. (2000). cDNA cloning of phosphoethanolamine N-methyltransferase from spinach by complementation in *Schizosaccharomyces pombe* and characterization of the recombinant enzyme. J. Biol. Chem. *275*, 14095–14101.

Palavalli, L.H., Brendza, K.M., Haakenson, W., Cahoon, R.E., McLaird, M., Hicks, L.M., McCarter, J.P., Williams, D.J., Hresko, M.C., and Jez, J.M. (2006). Defining the role of phosphomethylethanolamine N-methyltransferase from *Caenorhabditis elegans* in phosphocholine biosynthesis by biochemical and kinetic analysis. Biochemistry *45*, 6056–6065.

Peregrín-Alvarez, J.M., Sanford, C., and Parkinson, J. (2009). The conservation and evolutionary modularity of metabolism. Genome Biol. *10*, R63.

Pessi, G., Kociubinski, G., and Mamoun, C.B. (2004). A pathway for phosphatidylcholine biosynthesis in *Plasmodium falciparum* involving phosphoethanolamine methylation. Proc. Natl. Acad. Sci. USA *101*, 6206–6211.

Renslo, A.R., and McKerrow, J.H. (2006). Drug discovery and development for neglected parasitic diseases. Nat. Chem. Biol. *2*, 701–710.

Sheldrick, G.M. (2008). A short history of SHELX. Acta Crystallogr. A *64*, 112–122.

Sohlenkamp, C., López-Lara, I.M., and Geiger, O. (2003). Biosynthesis of phosphatidylcholine in bacteria. Prog. Lipid Res. *42*, 115–162.

Terwilliger, T.C. (2000). Maximum-likelihood density modification. Acta Crystallogr. D Biol. Crystallogr. *56*, 965–972.

Van Duyne, G.D., Standaert, R.F., Karplus, P.A., Schreiber, S.L., and Clardy, J. (1993). Atomic structures of the human immunophilin FKBP-12 complexes with FK506 and rapamycin. J. Mol. Biol. *229*, 105–124.

Walker, A.K., Jacobs, R.L., Watts, J.L., Rottiers, V., Jiang, K., Finnegan, D.M., Shioda, T., Hansen, M., Yang, F., Niebergall, L.J., et al. (2011). A conserved SREBP-1/phosphatidylcholine feedback circuit regulates lipogenesis in metazoans. Cell *147*, 840–852.

Wang, L., Yu, X., Hu, P., Broyde, S., and Zhang, Y. (2007). A water-mediated and substrate-assisted catalytic mechanism for *Sulfolobus solfataricus* DNA polymerase IV. J. Am. Chem. Soc. *129*, 4731–4737.

Watts, J.L. (2009). Fat synthesis and adiposity regulation in *Caenorhabditis elegans*. Trends Endocrinol. Metab. *20*, 58–65.

Weretilnyk, E.A., Smith, D.D., Wilch, G.A., and Summers, P.S. (1995). Enzymes of choline synthesis in spinach (response of phospho-base N-methyltransferase activities to light and salinity). Plant Physiol. *109*, 1085–1091.

Witty, M.J. (1999). Current strategies in the search for novel antiparasitic agents. Int. J. Parasitol. *29*, 95–103, discussion 113–114.

Zubieta, C., Ross, J.R., Koscheski, P., Yang, Y., Pichersky, E., and Noel, J.P. (2003). Structural basis for substrate recognition in the salicylic acid carboxyl methyltransferase family. Plant Cell *15*, 1704–1716.